Towards artificial photosynthesis : resolving supramolecular packing of artificial antennae chromophores through a hybrid approach

Thomas, B.

Chapter 1

Introduction and Methodology

1.1 Introduction

Spurred by worries over climate change and looming energy crisis, there is an increasing interest in mimicking natural photosynthesis for the conversion of solar energy into fuel.[1-4] Natural photosynthesis achieves solar to fuel conversion with photosynthetic antennae and reaction centers.[5-7] Biological systems are robust against random environmental fluctuations and can adapt to long-term evolutionary changes as well.[9] Their successful operation is based on a very limited set of functionally independent subsystems: protein complexes, subunits, and motifs dedicated to light harvesting,[4,10] charge separation and catalysis for extracting protons and electrons from water and for CO_2 reduction.[12] The most proficient light-harvesting antennae found in nature are chlorosomes, which are composed of a remarkably small set of interacting moderately sized organic dye molecules, mainly chlorophylls (MW~800).[4] Self-assembled bacteriochlorophyll (BChl) *c*, *d* or *e* organic dye pigments are preprogrammed for different tasks by adaptation of their structure, their interactions with the surrounding "responsive" matrix for the proper matching of time scales and length scales in the supramolecular biological organization.[13-17] Chlorophylls are sterically crowded in their side chains, and this makes for a flat energy landscape and molecules that can be easily distorted by packing effects to adapt the functional properties. These systems are frustrated by steric hindrance in the side chains. This leads to a flat energy landscape with respect to distortion of the molecule, where static and dynamic heterogeneity induced by the surrounding can have a very pronounced effect on the HOMO-LUMO gap and the redox potentials. As a result, one class of dye molecules can be used for different tasks, light harvesting, charge separation, water oxidation or proton reduction.

In the chlorosomes quantum delocalization is combined with symmetry breaking of the lowest exciton state to gain polaronic charge transfer character. Chlorophylls are spatially arranged in such a way to facilitate polaronic charge transfer character through the alignment of electric dipoles for a high dielectric susceptibility and charge transfer bias. This kind of chemical design is necessary to achieve oxidation of H_2O, which is a multielectron process. Moreover, the chlorophylls form two-dimensional sheets that allow for strong exciton overlap, enabling triplet exciton formation for photoprotection. Organic dyes in chlorosomes self-assemble in nanotubes and nanorods with coaxial cylinders and this serves as an inspiration for the design of nanodevices like modular tandem cells, or "artificial leaves" that perform light harvesting (at a time scale of ns), charge separation (ms) and multi-electron catalysis (ms).[18,19] Extensive studies have been performed in recent years on self-assembled chlorophylls in chlorosomes antennae, and have found that charge transfer states can be mixed effectively into exciton states when the building blocks have their dipole moments arranged in a parallel manner. Under ideal conditions, they can perform multi-electron photochemistry close to the thermodynamic limit for energy conversion and with nearly quantitative chemical yield, much better than any chemically engineered artificial system to date. Ultrafast, long-distance transmission of excitation energy in chlorophylls is achieved through the helical H-bonding chains and tight packing of BChls arising from π–π stacking in coaxial nanotubes. An induced misfit in the structural framework is achieved through chemical heterogeneity in the alkyl chains for optimization of the light-harvesting functionality. The various studies about the connection between the atomistic level and supramolecular organization of photosynthesis shows remarkable similarity in molecular nano architecture of the reaction center. To build a scaffold that replicates these nano architectures with biological functions like light harvesting, charge separation and catalysis, the challenge is to tune the different modules, which perform these functions in a controlled way. Since we know the functional entities involved in photosynthesis, it is possible to apply the well-known axiomatic design approach in the engineering world, which involves finding similar counterparts in organic and inorganic molecules.[9] The essence of axiomatic design in a solar fuel cell device is to build an artificial reaction center, which satisfies the

needs of light harvesting and charge separation. Functional requirements of artificial reaction centers are, absorption of photons to harvest light energy followed by transfer of the energy to the reaction center and then separation of charge to feed the catalyst.

Design parameters to achieve the functional requirements are matching the band gap of HOMO-LUMO with a wavelength of photons, suitable distance and energy gap for FRET, finely tuned reduction potential of the domain with a catalyst. Conformational entropy to mediate the conversions could be achieved through induced misfits. The morphology of the responsive matrix encodes the functional requirement and design parameters to achieve the system needs. As a first strategy to meet the system requirements, there has been much work on semi-synthetic dye molecules, where natural chlorophylls were chemically modified to reduce their chemical complexity and increase their stability.[20,21] The recent studies on chlorophylls and semi-synthetic dye molecules has provided us with a set of common characteristics for the programming and scaffolding of synthetic dye molecules for the design of nanodevices for artificial photosynthesis. Robustness of the synthetic antenna molecules can be used to match the design parameters with functional requirements.[22,23] In this thesis fused NDI-zinc salphen with a rigid supramolecular recognition motif formed out of salphen and a bichromophoric NMI functionalized perylene derivative with phenoxy spacers with the overlap of donors emission and acceptors absorption for FRET can be functionalized further for rationally designing the device. These molecules have remarkable chemical, thermal and photostability.

Insight into the packing obtained by the computational integration of two different bioimaging techniques, solid-state NMR and cryo-EM shows that chlorosomes contain well-ordered microdomains of self-assembled chlorophyll with *syn-anti* stacking mode. In the pursuit for nanodevices for solar to fuel conversion, a clear understanding about the packing serves to guide the design of new nanosized materials to meet the functional requirements for the design of a device compatible module for efficient light harvesting for the organic solar fuel cell. Recent advances in understanding about the chemical programming of chlorophyll cofactors for light harvesting, charge separation and driving catalysis at high redox potential in natural photosynthetic systems using MAS NMR

techniques provides a set of common denominators for the programming of artificial antenna complexes. The key point of this work is to transfer the body of knowledge acquired on chlorophyll tuning in photo biological systems to the artificial light harvesting component as a first step for the rational design of the device. Nature achieves functional complexity using a limited set of molecules, while the synthetic world has a lot of chemical diversity. The challenge that is addressed in this thesis is to take a set of molecules - perylene derivatives and DATZnS derivatives, and work towards the rational design of artificial light harvesting component and discover new concepts.

A cognizance about the packing will enable to steer the morphology in the desired direction. Moderately sized molecules like DATZnS derivatives and D1A2

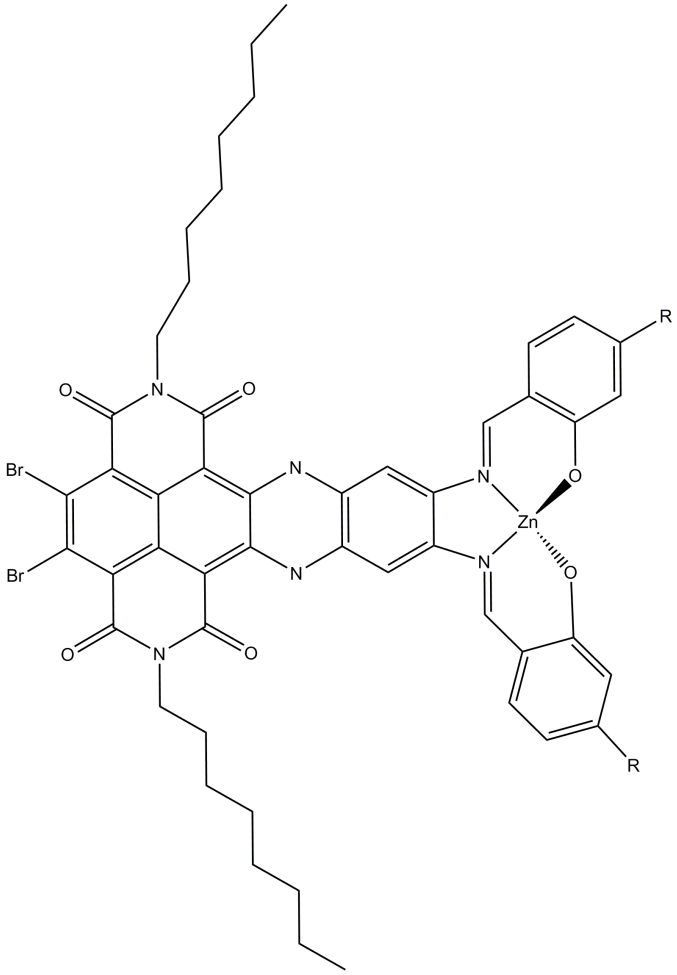

Figure 1.1 The structure of the DATZnS (R = 3′-NMe or 4H) derivative, a bichromophoric light harvesting antenna complex. The dipole moment is aligned along the principal axis of the molecule.

self-assemble to form supramolecular scaffolds with well-defined packing motifs that are planar aromatic. Chirality and asymmetry present in the molecules with protons on the conjugated aromatic molecules makes it suitable for the methodology that is discussed in this thesis. While asymmetry contributes to resolve the proton peaks in the spectrum, chirality leads to unique packing.

1.1.1 DATZnS derivatives

Core-expanded naphthalene diimide (cNDI) fused with a zinc bis-salicylimide phenylene (salphen) moiety is an alternative to porphyrin-based components used in supramolecular light-harvesting architectures (Figure 1.1).[5,24,25] Strategically incorporating metal-based supramolecular recognition motifs inside a chromophoric structure suggest the family of DATZnS derivatives as a new component for rationally designed light-harvesting assemblies.[26] The fused cNDI-zinc–salphen dyad behaves as one pigment and absorbs light between 600 and 750 nm with a modest Stokes shift.[26] Studies that were done on a homologue with orthogonal coordination of pyridine ligands to the rigid supramolecular scaffold of the DATZnS compound show that it does not undergo any change in its redox potentials or any internal excited state quenching and does not appreciably alter its excited state lifetime. Therefore it is expected that attachment of a catalyst as a ligand to the supramolecular scaffold limits the electronic influence of supramolecular interactions on the molecular orbitals involved in light absorption. This will give the flexibility to design it as a light-harvesting antenna complex for a solar fuel cell device.

1.1.2 Perylene derivative D1-A2

In the molecule D1A2, the energy donor naphthalene monoimide (NMI) has been attached to the 1, 7-bay-positions of the perylene derivative, thus leaving the peri positions free for further modification to design it as a device (Figure 1.2). The physical properties of perylene diimide dyes can be controlled by functionalization of the bay positions. Phenoxy spacers help to prevent π-π aggregation usually observed with perylene motifs and quenches the electron transfer from the naphthalene donor chromophores to the acceptor perylenes. Electrochemical properties and absorption spectra of D1 and A2 chromophores are independent of

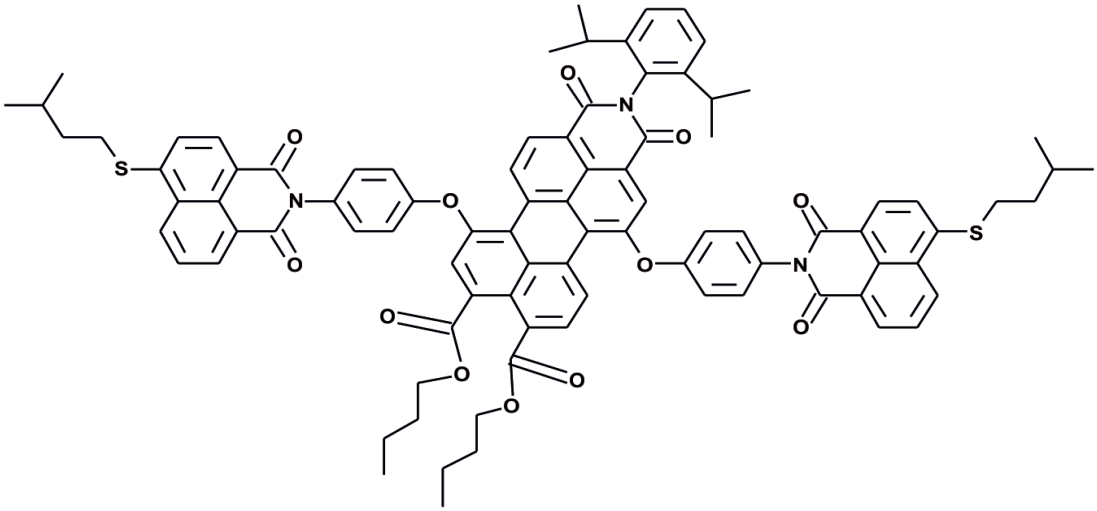

Figure 1.2 Structure of the perylene derivative with naphthalene monoimide (NMI) as bay substituents with phenoxy spacers. Overlap between the emission of NMI and absorption of perylene derivatives leads to transfer of energy through a FRET mechanism, which makes it an interesting antenna complex.

the coupling using the phenoxy spacer. Recent studies by Rajeev *et al*. show that the excited-state dynamics of D1A2, in toluene, has quantitative and ultrafast (ca. 1 ps) intramolecular excited energy transfer (EET) by the Forster mechanism. This arises due to the overlap of NMI's emission with absorption of perylene derivatives. Phenoxy coupling will impart high chemical stability and rigidity for the well-defined scaffold of the antenna molecules. The combination of an effective and fast energy transfer along with broad absorption in the visible region suggest that D1A2 or similarly designed dyes may fulfill a major role in the future development of organic supramolecular antenna systems.

1.2 Methodology

1.2. 1 NMR

NMR is a technology that has wide application in materials chemistry and biological chemistry to study the structure, dynamics and mechanisms of functions.

The NMR spin Hamiltonian is expressed as

$$\widehat{H} = \widehat{H}_z + \widehat{H}_D + \widehat{H}_{CS}. \quad (1.1)$$

Here $\widehat{H}_z$ is the Zeeman interaction, $\widehat{H}_{CS}$ is the chemical shielding term and $\widehat{H}_D$ represents the dipolar coupling. The Zeeman interaction is the interaction between the nuclear spins and the applied magnetic field. The Zeeman Hamiltonian is often represented as

$$\widehat{H}_Z = -\hat{\mu}B_0, \tag{1.2}$$

where $\hat{\mu} = \gamma\hbar\hat{I}$ indicates the nuclear magnetic momentum operator and B_0 is the applied magnetic field. Even though the Zeeman interaction is the predominant term in the spin Hamiltonian it contains little information about structure. The chemical shielding Hamiltonian, which is anisotropic, can be described by

$$\widehat{H}_{CS} = \gamma\hat{I}\sigma B_0\,, \tag{1.3}$$

where B_0 is the applied magnetic field, σ is the second rank chemical shielding tensor, and $\hat{I}$ is the nuclear spin operator.[27] The $\widehat{H}_{CS}$ depends on the orientation of the molecule with respect to the applied magnetic field, which makes it a rich source of information about the structure. The anisotropy is due to the fact that in a molecule the charge distribution is rarely spherically symmetric. Three principal values of chemical shielding tensor are described as isotropic value, anisotropy and, asymmetry of interaction. The isotropic average of the tensor is given by

$$\sigma_{iso} = \tfrac{1}{3}\left(\sigma_{xx}^{PAF} + \sigma_{yy}^{PAF} + \sigma_{zz}^{PAF}\right), \tag{1.4}$$

where σ^{PAF} indicates the principal values of the shielding tensor along the respective principal axis. The reduced anisotropy is given by

$$\delta = \sigma_{zz}^{PAF} - \sigma_{iso}, \tag{1.5}$$

and the shielding asymmetry is defined as

$$\eta = \left(\sigma_{yy}^{PAF} - \sigma_{xx}^{PAF}\right)\Big/\sigma_{zz}^{PAF}\,, \tag{1.6}$$

where σ_{iso} is the isotropic value, δ is the anisotropy and η is the asymmetry parameter.[28]

The dipolar coupling is based on the interaction of small local fields of the nuclear magnetic moments of different nuclei, and it is of two types, the homonuclear dipolar Hamiltonian between protons and the heteronuclear dipolar Hamiltonian between proton and carbon spins. The homonuclear dipolar Hamiltonian is represented as

$$\widehat{H}_{dd}^{homo} = -\sum_{i>j}\left[\left(\frac{\mu_0}{4\pi}\right)\frac{\gamma^2\hbar}{r_{ij}^3}\right].\frac{1}{2}\left(3cos^2\theta_{ij}-1\right)\left[3\hat{I}_z^i\hat{S}_z^j-\hat{I}^i.\hat{I}^j\right], \quad (1.7)$$

while the heteronuclear dipolar Hamiltonian is given by

$$\widehat{H}_{dd}^{hetero} = -\sum_{i>j}\left[\left(\frac{\mu_0}{4\pi}\right)\frac{\gamma^I\gamma^S\hbar}{r_{ij}^3}\right].\frac{1}{2}\left(3cos^2\theta_{ij}-1\right)2\hat{I}_z^i\hat{S}_z^j\,. \quad (1.8)$$

Here *i* and *j* label the spins, r_{ij} indicates the internuclear distance between the spins *i* and *j*, and θ_{ij} indicates the angle between the *i*-*j* internuclear vector. The strength of the dipolar coupling depends on γ, the distance between the nucleus and the orientation of the spin pairs with respect to the magnetic field.

The Larmor frequency refers to the rate of precession of the magnetic moment of the nuclei around the external magnetic field B_o according to

$$\omega_0 = \gamma B_0. \quad (1.9)$$

The chemical shift anisotropy arises due to the fact that in a molecule, the charge distribution is rarely spherically symmetrical. In solution NMR, a single isotropic chemical shift is observed due to fast molecular tumbling. In solids no such motion prevails, resulting in spectral broadening. High resolution in the spectra can be achieved through combined rotation and multiple-pulse spectroscopy (CRAMPS).[29,30] This involves a combination of multiple pulse techniques and magic angle spinning to suppress homonuclear dipolar interactions between the abundant spins and the chemical shift anisotropy. The dipolar coupling between nuclei depends on the geometric factor $(3cos^2\theta - 1)$ as shown

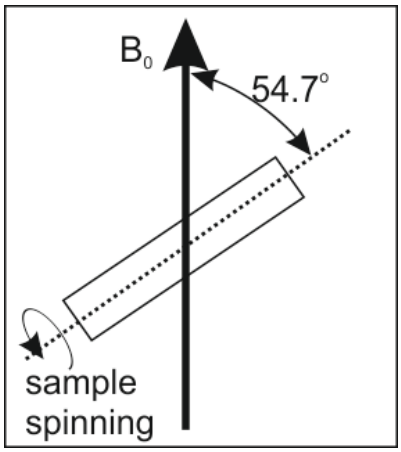

Figure 1.3 In a MAS experiment, the sample is finely powdered, packed tightly into a rotor and spun quickly around an axis at a magic angle of 54.75° with the magnetic field B_0.

in equation (1.7). Orienting the molecule at an angle of 54.7° and rotating at a high frequency helps to average the dipolar interaction (Figure 1.3).[31,32] Provided the rate of spinning is fast compared to homonuclear dipolar coupling linewidth, it will suppress to the formation of spinning sidebands and line broadening due to noncommuting terms in Hamiltonian (1.7).

1.2.1.1 Cross polarization

Low sensitivity and long spin-lattice relaxation times of dilute spin 1/2 nuclei can be overcome through cross polarization. Most dilute nuclei are in proximity of abundant nuclei like ^{1}H with a high gyromagnetic ratio. Polarization can hence be transferred from abundant nuclei to dilute nuclei through cross polarization.[33] A system of two nuclear spins, S and I are simultaneously irradiated with two rf fields B_{1I} and B_{1S} of frequencies ω_I and ω_S close to the Larmor frequencies. The so-called Hartmann-Hahn condition is satisfied when

$$|\omega_{1I}| = |\omega_{1S}|, \tag{1.10}$$

where $\omega_{1I} = -\gamma_{1I}B_{1I}$ and $\omega_{1S} = \gamma_S B_{1S}$.[34] During Hartmann-Hahn matching ^{1}H spins are locked along an effective field, while the ^{13}C spins can be locked on resonance in the xy-plane with a spin-lock pulse on the ^{13}C channel of the spectrometer. Polarization is transferred efficiently from ^{1}H spins to ^{13}C spins since it sets the energy gaps between the rotating frame spin states of ^{1}H and ^{13}C to be equal (Figure 1.4).

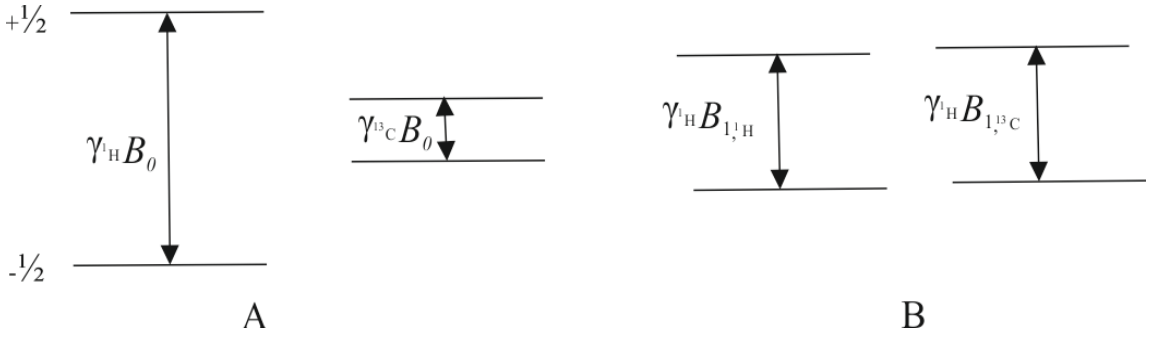

Figure 1.4 Energy levels of ^{1}H and ^{13}C spins in the laboratory frame (A) and the rotating frame (B). Polarization cannot be transferred in the laboratory frame due to energy mismatch. In the rotating frame, the splitting is determined by the *rf* field, and it is possible to tune the energy levels for the transfer of magnetization from ^{1}H to ^{13}C spins.

1.2.1.2 ^{1}H-^{13}C HETCOR and LGCP build up curves

Information about the internuclear distance between two spins can be deduced from the strength of the heteronuclear ^{1}H-^{13}C dipolar interactions. The cross polarization process is a mixture of coherent and incoherent transfer, but it is possible to extract the coherent transfer and measure the distance since the systems under study have sufficiently isolated spin pairs. For systems with ^{13}C at natural abundance, homonuclear ^{1}H decoupling at the LG condition restricts the transfer of polarization between ^{1}H spin pairs. Since ^{13}C is dilute, there are no ^{13}C-^{13}C interactions. Homonuclear dipolar interactions between protons can be averaged to zero by incorporating LG irradiation schemes in a CPMAS experiment (Figure 1.5A).[35,36] The LG technique involves irradiating the ^{1}H continuously with an off-resonance *rf*-field having frequency ω_1 with an off resonance value $\pm\Delta$LG. The LG condition is given by

$$\pm\Delta\mathrm{LG} = \omega_{\pm\Delta LG} - \gamma B_0 = \pm\frac{1}{2}\sqrt{2}\,|\omega_1|, \qquad (1.11)$$

where $\omega_1 = -\gamma B_1$. A series of multiple pulses is used to introduce the LG condition on the proton channel after a 90° pulse to suppress ^{1}H-^{1}H homonuclear dipolar interactions.

For the build-up curves, LGCP data were collected while increasing the CP contact time from 0.1 to 2 ms with increments of 0.1 ms. The LGCP build up curve

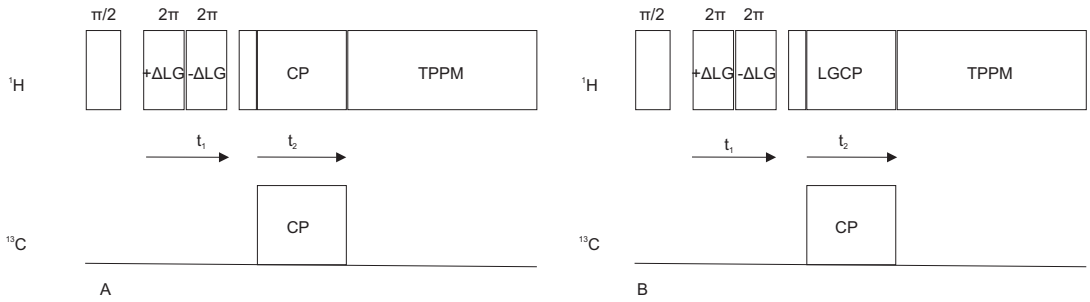

Figure 1.5 A) Pulse program used for ^{1}H-^{13}C LG HETCOR experiments. TPPM decoupling is used to suppress homonuclear coupling between ^{1}H spin pairs.[8] The ^{1}H magnetization is transferred to the ^{13}C spins via the dipolar coupling between ^{1}H and ^{13}C during a contact pulse (CP) applied simultaneously to both spins after a 90° pulse followed by LG conditions applied to the ^{1}H spins. B) Pulse program used for LGCP build up curve experiments. Here the LG condition is applied in the CP region, which suppresses the homonuclear coupling. This eventually helps to extract the LGCP build up curve between selected spin pairs.[11]

is obtained by plotting intensity against mixing time for each ^{13}C species (Figure 1.5B). The distance constraints can be obtained from the analysis of HETCOR and LGCP buildup curves. The LGCP build up curve can be simulated for various internuclear distances and then compared with experimental data to validate a proposed structure.[35]

1.3 Supramolecular crystallography

Packings consist of molecules arranged in a regular and quasi-periodic fashion. Analogous to the unit cell in crystals, packed supramolecular entities can have a repeating unit with intersecting edges labeled '*a*', '*b*' and '*c*' and angles between these edges labeled as '*α*', '*β*' and '*γ*'.[37,38] In addition to the unit cell parameters, space groups could be used to get an insight into the packing of these semicrystalline compounds in three dimension. The symmetry group of a configuration in space, usually in three dimensions is known as space group.[39,40] While there are many reflections in a crystalline structure due to long range order, packings have limited reflections due to limited correlation lengths, typically in the order of 50-100 unit cells, depending on the domain size.[41] Different diffraction patterns arise from the symmetry present in the molecule. Even with limited diffraction data we can still use Friedel's Law, which states that the intensities associated with two points opposite in reciprocal space, are almost equal: *I (h, k, l)*

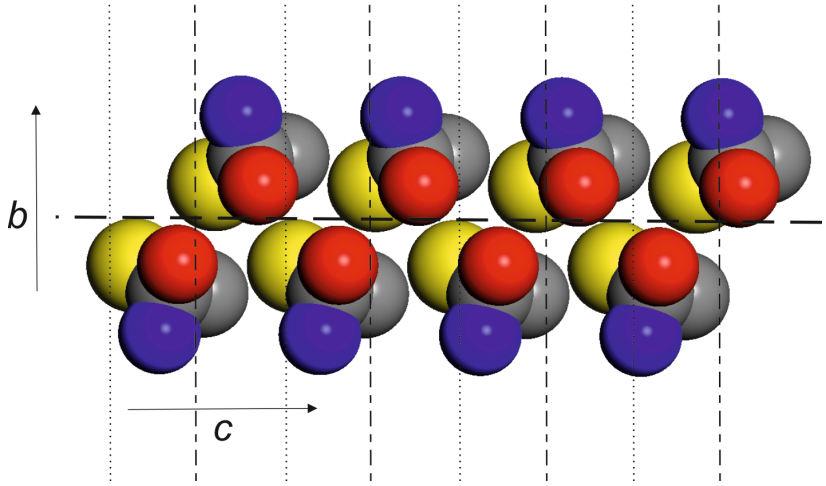

Figure 1.6 A 'c'- glide plane involves reflection on the plane containing the 'c' axis followed by translation along the same plane to accommodate steric hindrance. (adapted from http://pd.chem.ucl.ac.uk/pdnn/symm4/glide.htm)

≈ *I (-h, -k, -l)*.[42,43] Moreover, a pair of reflections with the indices *(h, k, l)* and *(-h, -k, -l)* is known as a Friedel pair.

Packing from the diffraction is determined mainly by two steps, it first involves finding the unit cell parameters.[44-47] The second step is to identify an approximate space group, which involves identifying possible screw axes and glide planes from reflection conditions in the diffraction pattern (Figure 1.6).[48] While screw axes imply rotation and an additional translation, the glide planes imply reflection and an additional translation. A screw axis has a one-dimensional reflection condition, while glide planes have two-dimensional reflection conditions. A twofold axis along the '*a*' axis leads to the reflection condition *h00:h=2n*. A glide plane perpendicular to the '*a*' axis results in the reflection condition *h=2n* onto the zonal plane *0kl*.

Most of the packing in organic molecules falls into three different crystal classes, they are triclinic, monoclinic and orthorhombic with $P2_1/c$, $P\bar{1}$, $P2_12_12_1$, $C2/c$ and $P2_1$ as the preferred space groups.[49] Space groups $P1$, $P\bar{1}$, $P1m$, $P12/m1$ and $P121/m1$ do not have any reflection condition. Polar space groups are $P1$, $P2$, $P21$ and $C2$. The CP/MAS NMR spectrum helps to identify the presence of symmetry in the molecule, which gives information about identical sites present in the packing. Polymorph analysis could be used to narrow down the possible crystal structures.[50,51] The number of molecules in the unit cell can be calculated using the equation $z = \frac{\rho * V}{M}$ where ρ is the density of the sample, V is the volume of the unit cell and M is the molecular weight.[20,21,50,52] This work is based on the assumption that the number of molecules in the unit cell should be in correspondence with the number of identical sites from the mathematical operators in the space group, taking into account the symmetry of the molecule. This will allow predominant interplay between bottom up and top down packing constraints. Geometrical optimization helps to converge on a reasonable packing. Furthermore the packing could be validated with simulation of chemical shifts, LGCP build up curves and diffraction patterns.[35,37,53,54] In the later stage, the methodology involving the computational integration of electron diffraction, CP/MAS NMR and modelling could be extended to find the packing in other systems that are heterogeneous in nature (Figure 1.7).

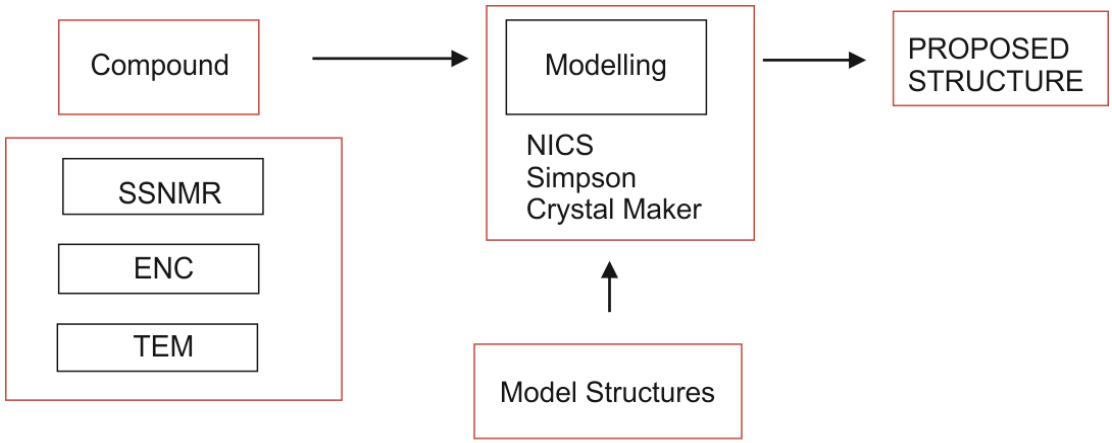

Figure 1.7 Schematic representation of supramolecular crystallography. The concept here is to reduce the uncertainty of the model by reasoning from first principles using the available data from CP/MAS NMR, ENC, and TEM. The logic behind the reconstruction of a model is to search for global packing that can reproduce commonalities in the observed data through simulation.

The scope of this thesis is to perform and develop a methodology for the magnetic resonance and electron diffraction analyses for the evidence-based design of device compatible modules for light harvesting. In this thesis, a concept for solving the packing of pseudocrystalline supramolecular dye assemblies in the solid-state at natural abundance by using MAS NMR in conjunction with electron diffraction is illustrated. This involves the smart use of a glide plane to accommodate steric hindrance to get packing with low energy and high density, which provides a design strategy for solar fuel cell device.

Chapter 2 describes how CP/MAS NMR in combination with cryo-EM can be applied to elucidate the structure of pseudo-crystalline DATZnS(3′-NMe) which forms antiparallel stacking with the $P2/c$ space group. MAS NMR and quantitative chemical shift calculations provide information about the C_2 symmetry and selective distance constraints. Systematic absences from the diffraction pattern give details about the screw axis and glide plane. The electron diffraction pattern and LGCP build up curve between specific pairs were simulated to validate the proposed packing.

In **Chapter 3**, the latest state of the art in electron diffraction, which is the ENC, is used to get the unit cell parameters and space group. This involves rotation of the crystal with continuous exposure to the electron beam over a limited angle.

The nonzero scattering in reciprocal space obtained by ENC is converted into electron density using Phaser molecular replacement with the help of a rigid trial model. Intermolecular correlations help to converge on a centrosymmetric dimer and then bay substituents were grafted to this basic building motif followed by modeling of the structure.[55] Finally the packing is validated with MAS NMR.

A homology modeling approach was used in **Chapter 4**. Here the DATZnS(3'-NMe) in chapter 2 is used as a starting model. MAS NMR and limited data from TEM were feed into the modeling to converge upon an antiparallel packing. This provides insight on how to steer the packing from antiparallel into parallel by using functional groups and steric constraints. This paves the way for evidence based chromophoric design of antenna motifs for artificial photosynthesis.

Finally in **chapter 5**, a summary is given about the results reported in this thesis. In addition, a brief description about the future developments, needed with design of the device and in the field of structural analysis, is given.

References

(1) Purchase, R. L.; de Groot, H. J. M. *Interface Focus* **2015**, *5, 20150014*.

(2) Gust, D.; Moore, T. A.; Moore, A. L. *Accounts of Chemical Research* **2009**, *42*, 1890.

(3) Scholes, G. D.; Fleming, G. R.; Olaya-Castro, A.; van Grondelle, R. *Nat Chem* **2011**, *3*, 763.

(4) Croce, R.; van Amerongen, H. *Nat Chem Biol* **2014**, *10*, 492.

(5) Fernando, R.; Etheridge, F.; Muller, E.; Sauve, G. *New Journal of Chemistry* **2015**, *39*, 2506.

(6) Bensaid, S.; Centi, G.; Garrone, E.; Perathoner, S.; Saracco, G. *ChemSusChem* **2012**, *5*, 500.

(7) Janna Olmos, J. D.; Kargul, J. *The International Journal of Biochemistry & Cell Biology* **2015**, *66*, 37.

(8) van Rossum, B. J.; Förster, H.; de Groot, H. J. M. *Journal of Magnetic Resonance* **1997**, *124*, 516.

(9) Thomas, J. D.; Lee, T.; Suh, N. P. *Annual Review of Biophysics and Biomolecular Structure* **2004**, *33*, 75.

(10) Demmig-Adams, B.; Adams, W. W. *Nature* **2000**, *403*, 371.

(11) Bielecki, A.; Kolbert, A. C.; Levitt, M. H. *Chemical Physics Letters* **1989**, *155*, 341.

(12) Alia, A.; Buda, F.; Groot, H. J. M. d.; Matysik, J. *Annual Review of Biophysics* **2013**, *42*, 675.

(13) Furumaki, S.; Vacha, F.; Hirata, S.; Vacha, M. *ACS Nano* **2014**, *8*, 2176.

(14) Jochum, T.; Reddy, C. M.; Eichh; xf; fer, A.; Buth, G.; Szmytkowski, J.; x; drzej; Kalt, H.; Moss, D.; Balaban, T. S. *Proceedings of the National Academy of Sciences of the United States of America* **2008**, *105*, 12736.

(15) Matenova, M.; Lorelei Horhoiu, V.; Dang, F.-X.; Pospisil, P.; Alster, J.; Burda, J. V.; Silviu Balaban, T.; Psencik, J. *Physical Chemistry Chemical Physics* **2014**, *16*, 16755.

(16) Saga, Y.; Akai, S.; Miyatake, T.; Tamiaki, H. *Bioconjugate Chemistry* **2006**, *17*, 988.

(17) Möltgen, H.; Kleinermanns, K.; Jesorka, A.; Schaffner, K.; Holzwarth, A. R. *Photochemistry and Photobiology* **2002**, *75*, 619.

(18) Kalyanasundaram, K.; Graetzel, M. *Current Opinion in Biotechnology* **2010**, *21*, 298.

(19) Young, K. J.; Martini, L. A.; Milot, R. L.; Iii, R. C. S.; Batista, V. S.; Schmuttenmaer, C. A.; Crabtree, R. H.; Brudvig, G. W. *Coordination chemistry reviews* **2012**, *256*, 2503.

(20) Ganapathy, S.; Oostergetel, G. T.; Wawrzyniak, P. K.; Reus, M.; Gomez Maqueo Chew, A.; Buda, F.; Boekema, E. J.; Bryant, D. A.; Holzwarth, A. R.; de Groot, H. J. M. *Proceedings of the National Academy of Sciences* **2009**, *106*, 8525.

(21) Ganapathy, S.; Sengupta, S.; Wawrzyniak, P. K.; Huber, V.; Buda, F.; Baumeister, U.; Würthner, F.; de Groot, H. J. M. *Proceedings of the National Academy of Sciences* **2009**, *106*, 11472.

(22) Dubey, R. K.; Inan, D.; Sengupta, S.; Sudholter, E. J. R.; Grozema, F. C.; Jager, W. F. *Chemical Science* **2016**, *7*, 3517.

(23) Dubey, R. K.; Knorr, G.; Westerveld, N.; Jager, W. F. *Organic & Biomolecular Chemistry* **2016**, *14*, 1564.

(24) Rombouts, J. A.; Ravensbergen, J.; Frese, R. N.; Kennis, J. T. M.; Ehlers, A. W.; Slootweg, J. C.; Ruijter, E.; Lammertsma, K.; Orru, R. V. A. *Chemistry – A European Journal* **2014**, *20*, 10185.

(25) Ponnuswamy, N.; Stefankiewicz, A. R.; Sanders, J. K. M.; Pantoş, G. D. In *Constitutional Dynamic Chemistry*; Barboiu, M., Ed.; Springer Berlin Heidelberg: Berlin, Heidelberg, **2012**, 217.

(26) Tong, L. H.; Pengo, P.; Clegg, W.; Lowe, J. P.; Raithby, P. R.; Sanders, J. K. M.; Pascu, S. I. *Dalton Transactions* **2011**, *40*, 10833.

(27) Saitô, H.; Ando, I.; Ramamoorthy, A. *Progress in nuclear magnetic resonance spectroscopy* **2010**, *57*, 181.

(28) Blümich, B. *Advanced Materials* **1996**, *8*, 186.

(29) Schaefer, J.; Stejskal, E. O. *Journal of the American Chemical Society* **1976**, *98*, 1031.

(30) Dec, S. F.; Bronnimann, C. E.; Wind, R. A.; Maciel, G. E. *Journal of Magnetic Resonance (1969)* **1989**, *82*, 454.

(31) Andrew, E. R.; Bradbury, A.; Eades, R. G. *Nature* **1958**, *182*, 1659.

(32) Lowe, I. J. *Physical Review Letters* **1959**, *2*, 285.

(33) Hartmann, S. R.; Hahn, E. L. *Physical Review* **1962**, *128*, 2042.

(34) Lee, M.; Goldburg, W. I. *Physical Review* **1965**, *140*, A1261.

(35) Ladizhansky, V.; Vega, S. *Journal of the American Chemical Society* **2000**, *122*, 3465.

(36) Fukuchi, M.; Ramamoorthy, A.; Takegoshi, K. *Journal of magnetic resonance (San Diego, Calif. : 1997)* **2009**, *196*, 105.

(37) Vosegaard, T.; Tošner, Z.; Nielsen, N. C. In *eMagRes*; John Wiley & Sons, Ltd: 2007.

(38) Kremer, F. In *Zeitschrift für Physikalische Chemie* **1997**, *200*, 281.

(39) Opgenorth, J.; Plesken, W.; Schulz, T. *Acta Crystallographica Section A* **1998**, *54*, 517.

(40) Hestenes, D.; Holt, J. W. *Journal of Mathematical Physics* **2007**, *48*, 023514.

(41) Ganapathy, S.; Oostergetel, G. T.; Reus, M.; Tsukatani, Y.; Gomez Maqueo Chew, A.; Buda, F.; Bryant, D. A.; Holzwarth, A. R.; de Groot, H. J. M. *Biochemistry* **2012**, *51*, 4488.

(42) Bijvoet, J. M.; Peerdeman, A. F.; van Bommel, A. J. *Nature* **1951**, *168*, 271.

(43) Serneels, R.; Snykers, M.; Delavignette, P.; Gevers, R.; Amelinckx, S. *physica status solidi (b)* **1973**, *58*, 277.

(44) Martineau, C. *Solid State Nuclear Magnetic Resonance* **2014**, *1*,63.

(45) Ripmeester, J. A.; Wasylishen, R. E. *CrystEngComm* **2013**, *15*, 8598.

(46) Ashbrook, S. E.; McKay, D. *Chemical Communications* **2016**, *52*, 7186.

(47) Doerr, A. *Nat Meth* **2006**, *3*, 6.

(48) Kalman, A.; Argay, G.; Fabian, L.; Bernath, G.; Fulop, F. *Acta Crystallographica Section B* **2001**, *57*, 539.

(49) Pidcock, E. *Chemical* Communications **2005**, 3457.

(50) Baias, M.; Dumez, J.-N.; Svensson, P. H.; Schantz, S.; Day, G. M.; Emsley, L. *Journal of the American Chemical Society* **2013**, *135*, 17501.

(51) Cross, W. I.; Blagden, N.; Davey, R. J.; Pritchard, R. G.; Neumann, M. A.; Roberts, R. J.; Rowe, R. C. *Crystal Growth & Design* **2003**, *3*, 151.

(52) Baias, M.; Widdifield, C. M.; Dumez, J.-N.; Thompson, H. P. G.; Cooper, T. G.; Salager, E.; Bassil, S.; Stein, R. S.; Lesage, A.; Day, G. M.; Emsley, L. *Physical Chemistry Chemical Physics* **2013**, *15*, 8069.

(53) Kohn, S. C. *Terra Nova* **1995**, *7*, 554.

(54) Bak, M.; Rasmussen, J. T.; Nielsen, N. C. *Journal of Magnetic Resonance* **2000**, *147*, 296.

(55) McCoy, A. J. *Acta Crystallographica Section D: Biological Crystallography* **2007**, *63*, 32.